NJC

Accepted Manuscript

This is an *Accepted Manuscript*, which has been through the Royal Society of Chemistry peer review process and has been accepted for publication.

Accepted Manuscripts are published online shortly after acceptance, before technical editing, formatting and proof reading. Using this free service, authors can make their results available to the community, in citable form, before we publish the edited article. We will replace this *Accepted Manuscript* with the edited and formatted *Advance Article* as soon as it is available.

You can find more information about *Accepted Manuscripts* in the Information for Authors.

Please note that technical editing may introduce minor changes to the text and/or graphics, which may alter content. The journal's standard Terms & Conditions and the Ethical guidelines still apply. In no event shall the Royal Society of Chemistry be held responsible for any errors or omissions in this *Accepted Manuscript* or any consequences arising from the use of any information it contains.

ROYAL SOCIETY OF CHEMISTRY

www.rsc.org/njc

Amphiphilic Unsymmetrically-Substituted Porphyrin Zinc Derivatives: Synthesis, Aggregation Behavior in the Self-Assemblied Films and NO_2 Sensing Properties

Yanling Wu,[a] Pan Ma,[c] Shanshan Liu[a] and Yanli Chen[a,b*]

[a] Shandong Provincial Key Laboratory of Fluorine Chemistry and Chemical Materials, School of Chemistry and Chemical Engineering, University of Jinan, Jinan 250022, China

[b] School of Science, China University of Petroleum (East China), Qingdao 266580, China.

[c] Jinan Academy of Agricultural Sciences, Jinan 250316, China

* Corresponding author. E-mail: chm_chenyl@ujn.edu.cn; yanlichen@upc.edu.cn

Tel: +86 (0)531 8973 6150

Abstract

Two novel amphiphilic porphyrin derivatives 5-(Benzo-(4-(2-(2-hydroxy)ethoxy)ethoxy))-10,15,20-triphenylporphyrinato zinc complex [ZnT($OC_2H_4OC_2H_4OH$)PP] (**1**) and 5-(Benzo-(4-(2-(4,10-N,N-15-Crown-5)ethoxy))-10,15,20-triphenylporphyrinato zinc complex [ZnT(OC_2H_4NN15C5)PP] (**2**) were designed , synthesized, and characterized by a range of spectroscopic methods. Their electrochemistry has been studied by differential pulse voltammetry (DPV). Highly ordered films of **1** and **2** were fabricated by a solution-based quasi-Langmuir-Shäfer (QLS) technique, and were characterized by electronic absorption spectra, IR, X-ray diffraction, atomic force microscopy (AFM) and current–voltage (*I*–*V*) measurements. Experimental results revealed that *J*-type aggregates have been formed in the QLS film of **1** and **2**. The crystallinity and general molecular order in the film of **1** are improved more effectively than those of **2** due to its stronger intermolecular interactions. Furthermore, the conductivity of the QLS film of **1** was approximately 1 order of magnitude larger than that of **2**. This indicates significant effect of peripheral groups on conducting behavior of porphyrins. In addition, the gas sensing behavior of the QLS films of **1** and **2** toward electron acceptor gas, NO_2, was investigated in the concentrations of 200 and 800 ppm, respectively. The sensitivity, stability, reproducibility follows the order **1** > **2**, revealing the effect of the intermolecular interaction, film structure/morphology, and low-lying LUMO energy level on sensing performance. Unexpectedly, a decreased current response towards NO_2 for the QLS films of both **1** and **2** were obtained for the first time, which unambiguously demonstrated the n-type semiconducting nature for **1** and **2**. The present result represents not only the first example of n-type metalloporphyrin-based thin solid films obtained by a solution-based method, but more importantly provides an efficient way to enhance the performance of n-channel organic semiconductors through the combination of molecular design and film fabrication technique.

Keywords: Porphyrins, NO_2 sensor, Conductivity, Organic semiconductors

1 Introduction

As the representatives of functional molecular materials with large conjugated electronic molecular structures, metalloporphyrins and their derivatives, due to properties such as great processability, high thermal and chemical stability and rich substitution chemistry, are one of the most promising candidates for modern opto-electronic devices such as dye-sensitized solar cells, organic light-emitting diodes, field effect transistors, optical recording and gas sensors.[1-8] For most of the applications, the properties of the molecular devices are closely related to the microstructures of the solid films. Although many strategies have been explored to control the organization of porphyrin-based building blocks into unique microstructures with different morphology such as fibers, wires, channels, giant micelles, two-dimensional sheets, and cages.[9,10] It is still a challenge for chemists and material scientists to construct porphyrin-based nano-assembly into a highly ordered film-structure using a low-cost, solution-based method through the combination of molecular design and programming the supramolecular interaction.

Nowadays, the interest in developing gas detectors having porphyrin derivates as the chemically sensitive component of chemical/conductometric transduction systems is steadily increasing, since their electrical properties change upon exposure to oxidizing gases such as NO_2.[11-13,14] It has been found that the synergistic effect of the molecular interactions (such as Van der Waals and hydrogen bonding) among porphyrins in the aggregates and the intermolecular porphyrin-analyte coordination interactions to determine the sensing performances of the porphyrins.[15] Many efforts have been made to clarify the relationships between the molecular ordering in the film of the porphyrins and the sensing performances. For example, Kerdcharoen et al. found that an annealed MgTPP film with improved film-structure exhibited better response to VOCs than that of non-annealed MgTPP film.[16] Valli et al. reported that the conductivity of the porphyrins compounds attached with electron withdrawing substituents, which exhibit n-type semiconducting behavior, increases in the presence of electron donor gases such as NH_3 and decreases in electron acceptor gases such as O_2 and NOx.[11] The sensitivity of porphyrins towards analytes significantly improves, when the functionalization on the periphery of the macrocycle or the central metal atom inside the porphyrin core is modified.[11]

On the other hand, the thin films can be produced by a variety of techniques, such as vacuum sublimation, electron-beam evaporation and simple solution-processing methods. Soluble molecules can be deposited by solution-processing methods, including casting techniques, such as drop casting, spin-coating, or via layer-by-layer assembly techniques such as the Langmuir–Blodgett (LB: vertical transfer), Langmuir-Shäfer (LS: horizontal transfer) and Quasi-Langmuir–Shäfer (QLS) protocols, the surface-assisted self-assembly technique etc. LB, LS and QLS techniques allow obtaining films with good thickness control and offer the possibility to easily produce multilayer structured films by applying an external compression force at air–water interface. In particular, QLS method developed by Bouvet's group requires no sophisticated set-up with a lower cost relative to LS , which has been employed to obtain the well-organized films of amphiphilic molecules at air–water interface.[17-19,28] To get an insight into the gas-sensing nature of amphiphilic metalloporphyrin molecules, in the present paper, we describe the synthesis and electrochemical properties of two novel amphiphilic porphyrin derivatives 5-(Benzo-(4-(2-(2-hydroxy)ethoxy)ethoxy))-10,15,20-triphenylporphyrinato zinc complex [ZnT($OC_2H_4OC_2H_4OH$)PP] (**1**) and 5-(Benzo-(4-(2-(4,10-N,N-15-Crown-5)ethoxy))-10,15,20-triphenylporphyrinato zinc complex [ZnT(OC_2H_4NN15C5)PP] (**2**), Scheme 1. Highly ordered films of **1** and **2** were fabricated by a solution-based quasi-Langmuir-Shäfer (QLS) technique. The electrical conductivity of the film of **1** was measured to be approximately 1 orders of magnitude larger than that of the film of **2**. The gas sensing behavior of the QLS films of **1** and **2** toward NO_2 was investigated in the concentrations of 200 and 800 ppm.

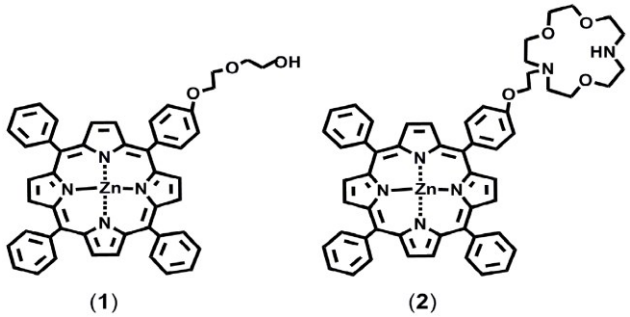

(**1**) (**2**)

Scheme 1 Schematic structures of [ZnT($OC_2H_4OC_2H_4OH$)PP] (**1**) and [ZnT(OCH_2CH_2NN15C5)PP] (**2**).

2 Results and discussion

2.1 Molecular design, synthesis, and electrochemistry

5-(Benzo-(4-(2-(2-hydroxy)ethoxy)ethoxy))-10,15,20-triphenylporphyrinato zinc complex [ZnT($OC_2H_4OC_2H_4OH$)PP] (**1**) was synthesized according to a recently developed procedure.[20] For the purpose of comparative study, 5-(Benzo-(4-(2-(4,10-N,N-15-Crown-5)ethoxy))-10,15,20-triphenylporphyrinato zinc complex [ZnT(OC_2H_4NN15C5)PP] (**2**) was also prepared following published methods.[20]

All the newly prepared porphyrinato zinc compounds gave satisfactory test results. The Matrix-assisted laser desorption/ionization time-of-flight (MALDI-TOF) spectra of all these compounds showed the molecular ion $(M)^+$ signals with correct isotopic pattern, As shown in Fig. S1. The ^{1}H NMR spectra of newly prepared porphyrinato zinc compounds **1**–**2** were recorded in $CDCl_3$ at room temperature (see Electronic Supplementary Information).

The electrochemical behavior of the two porphyrinato zinc compounds **1**–**2** was investigated using differential pulse voltammetry (DPV) in CH_2Cl_2. These compounds display one one-electron reduction labelled as Red_1 and three one-electron oxidation (Oxd_1–Oxd_3) within the electrochemical window of CH_2Cl_2 under the present conditions. The half-wave redox potential values vs. SCE (standard calomel electrode) are summarized in Table 1. Representative differential pulse voltammograms for **1** and **2** are displayed in Fig. 1. Their highest occupied molecular orbital (HOMO) and lowest unoccupied molecular orbital (LUMO) energy levels were estimated to be about -5.81, -3.88 eV for **1** and -5.21, -3.60 eV for **2**, respectively, based on DPV measurements.[21]

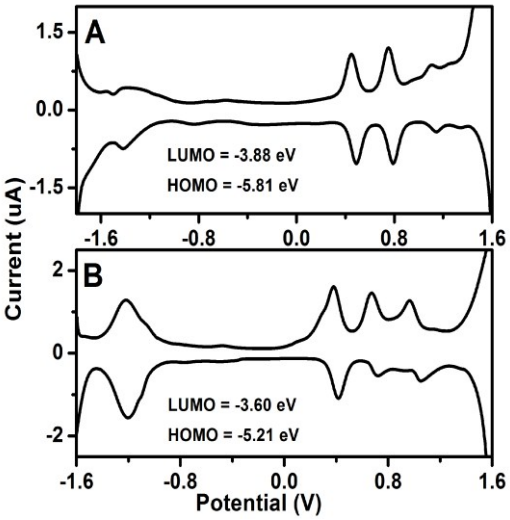

Fig. 1 Differential pulse voltammograms of **1** (A) and **2** (B) in CH_2Cl_2 containing 0.1 M [NBu_4][ClO_4] at a scan rate of 20 $mV{\cdot}s^{-1}$, respectively.

Table 1 Half-wave redox potentials of [ZnT($OC_2H_4OC_2H_4OH$)PP] (**1**) and [ZnT(OC_2H_4NN15C5)PP] (**2**) (V vs. SCE) in CH_2Cl_2 containing 0.1 mol dm^{-3} [Bu_4N][ClO_4] together with the HOMO and LUMO levels of **1** and **2**.

Compound	Red_1/V	Oxd_1/V	Oxd_2/V	Oxd_3/V	HOMO/eV	LUMO/eV	$\Delta E^o_{1/2}$/eV
1	-1.46	0.47	0.77	1.12	-5.81	-3.88	1.93
2	-1.21	0.38	0.67	0.97	-5.21	-3.60	1.59

[a] Calculated from empirical formula of HOMO =-(Oxd_1+ 4.44 eV); LUMO =-(Red_1+ 4.44 eV)[21]

[b] $\Delta E^o_{1/2}$= Oxd_1–Red_1, i.e. the HOMO LUMO gap of corresponding molecule

2.2 UV-vis absorption spectra

The electronic absorption spectra of the two unsymmetrical porphyrinato zinc derivatives **1** and **2** were recorded in chloroform, Fig. 2 (solid line). As shown in Fig 2, the compounds **1** and **2** show a characteristic Soret band at ca. 420 and 421 nm, respectively. In addition, two satellite Q-bands at 548 and 587 nm are observed for **1** and 553, 602 nm for **2**.

These observations are in line with the reports for metalloporphyrins.[22,23] After being fabricated into the QLS film, the UV-vis absorption spectra of **1** and **2** exhibited the remarkable red-shifts, by comparing the absorption in solution, from 420, 548, 587 nm to 437, 561, 601 nm for **1** and from 421, 553, 602 nm to 440, 563, 604 nm for **2**, respectively, Fig. 2 (dashed line). This indicates the formation of *J*-type molecular packing structure (*J* aggregation) due to the strong exciton coupling between the neibouring molecules in the films of **1** and **2**.[24,25] Furthermore, the larger red-shifts of absorption bands were achieved in QLS films of **1** than those of **2**, implying an effect of the substituent group incorporated onto the meso-substituted phenyl group of porphyrin ring on the intermolecular interaction in solid films. This is also supported by the orientation angle (dihedral angle) revealed for the porphyrin ring with respect to the substrate. As shown in Fig. S2 and Table S1 (ESI),[26] the orientation angles of porphyrin rings to the quartz plate surface in the QLS films of [ZnT($OC_2H_4OC_2H_4OH$)PP] (**1**) and [ZnT(OC_2H_4NN15C5)PP] (**2**) are calculated to be 48.7° and 34.5°, respectively, according to polarized UV–vis measurement. This indicates again that molecules of both **1** and **2** take a slipped co-facial stacking mode with an ''edge-on'' configuration in the QLS films. Note that a larger orientation angle of porphyrin ring with a relative larger red-shift of absorption bands in the film of **1** was resulted from more effective intermolecular interaction in the *J* aggregates together with the intense intramolecular π–π stacking, which were expected to provide the π electrons with an extensive area for delocalization in the film of **1**. This forms the most basic necessary characteristics for an organic semiconductor with good charge transport ability.[27,28]

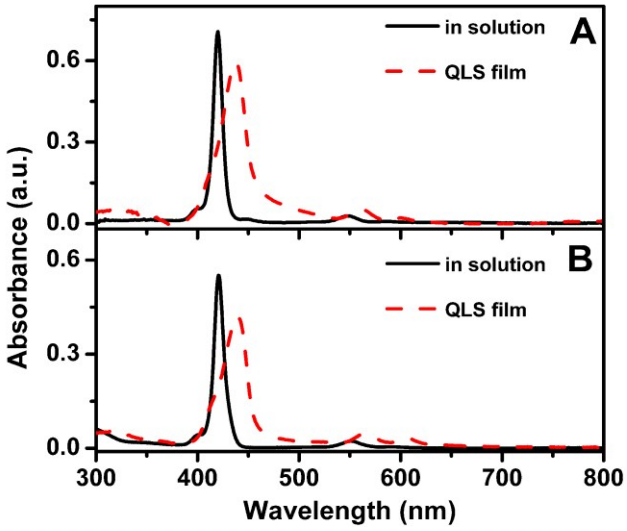

Fig. 2 UV–vis absorption spectra of **1 (A)** and **2** (B) in $CHCl_3$ solution (solid line) and the QLS films (dashed line).

2.3 IR spectra

The IR spectra of [ZnT($OC_2H_4OC_2H_4OH$)PP] (**1**) and [ZnT(OC_2H_4NN15C5)PP] (**2**) bulk samples together with their QLS films are compared in Fig. 3. The positions of the peak frequencies in the the high-frequency region of 2800–3000 cm^{-1}, which feature the symmetric and asymmetric C–H stretching from CH_2 groups ($\nu_s(CH_2)$ and $\nu_a(CH_2)$) in the side chains, provide insight into the intermolecular environment of the alkoxy chains of **1** and **2** in the QLS films relative to the corresponding bulk samples. Previous IR studies have shown that the location of these peaks is a sensitive indicator for the extent of the lateral interactions.[17,29,30] For example, the peak frequencies at 2927 and 2871 cm^{-1} in the bulk-phase of **1**, which are attributed to the $\nu_a(CH_2)$ and $\nu_s(CH_2)$ stretching modes from the (O)C–H vibration of the ethoxyglycol side chain, shifted to lower positions at 2925 and 2853 cm^{-1} in the QLS film of **1**, Fig. 3A. The same phenomena could also be observed for the peak frequencies of **2** from (O)C–H vibration of ethoxy side chain with the $\nu_a(CH_2)$ and $\nu_s(CH_2)$ modes at 2927 and 2865 cm^{-1} in bulk-phase and 2925 and 2853 cm^{-1} in the QLS film. A definite trend toward lower peak frequencies of the QLS film than those of bulk-phase for either **1** or **2** indicated the side chains are more ordered in the films than those in bulk-phases.[31,32]

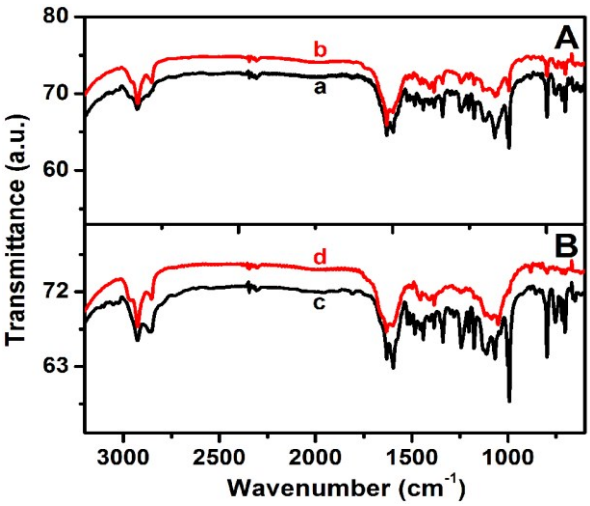

Fig. 3 IR spectra of **1** (A) and **2** (B) in the bulk samples (a and c) and the QLS films (b and d), respectively.

2.4 X-Ray diffraction patterns

The quality of the thin films as well as the preferred molecular orientation has been assessed using the out-of-plane (OOP) X-ray diffraction (XRD) technique. Both compounds **1** and **2** deposited on SiO_2 substrates give one distinct diffraction peak in their low angle region, respectively, Fig. 4, indicating that the molecules of either **1** or **2** are uniformly oriented relative to the substrate plane with a layered structure in the films.[33,19] The OOP XRD of the QLS film of **1** and **2** exhibits the (001) Bragg peak at 2θ = 7.24° and 5.44°, respectively, corresponding to a periodic spacing distance of 1.22 and 1.62 nm. Judging from a geometry-optimized, molecular length of **1** and **2** (1.59 and 2.53 nm), the tilt angle relative to the substrate of 50.1° and 39.8° are estimated for **1** and **2**, respectively. This corresponds well with the result of polarized UV–vis spectra, indicating again that the molecules both **1** and **2** take a slipped co-facial stacking mode with an ''edge-on'' configuration in the QLS films. In addition, the XRD pattern for the QLS films of both **1** and **2** also present one sharp refraction at 0.31 nm, which is attributed to the π–π stacking distance between tetrapyrrole cores of neighboring porphyrin molecules along the direction perpendicular to the tetarpyrrole rings.[34] It is worth noting that, in comparsion with that of **2**, the (001) diffraction peak with increased intensity and sharpening in the low-angle region for the film of **1** was obtained, Fig. 4, which indicates the obviously improved molecular ordering and enhanced crystallinity in the film of **1** relative to that of **2**. The better crystallinity in the QLS films of **1** compared to that of **2** can be related to not only improved co-planarity by the unique co-facially stacking structure, but more importantly the minimization of steric repulsions by the substituent ethoxyglycol side chain (which results in a highly ordered and denser molecular packing and aligned nature of **1** in the films).

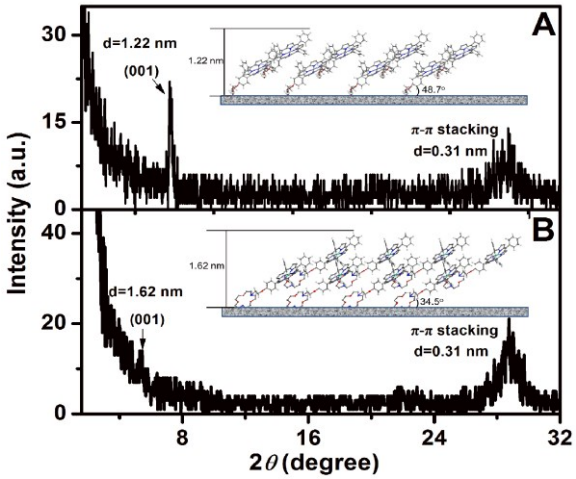

Fig. 4 X-ray patterns for the QLS films of **1** (A) and **2** (B) deposited on SiO_2 substrates. The insets are schematic packing modes of the molecules **1** and **2** in the QLS film, respectively.

2.5 Morphology of the QLS film

The morphology of the QLS films of **1-2** was also characterized by atomic force microscopy (AFM). The surface of the QLS film of **1** presents a granular structure with uniform grain crystallites, approximately 70 nm in diameter, whereas that of **2** exhibits nanoparticles with the average diameter of ca. 60 nm, Fig. 5. The increase in both the grain size and the grain crystallinity would be beneficial to the charge transport in the QLS film of **1** relative to that of **2**.

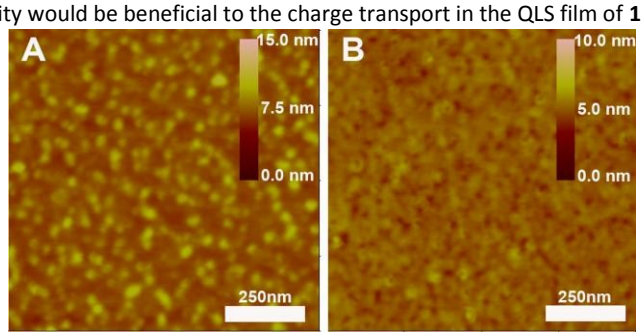

Fig. 5 AFM images of the QLS films **of 1** (A) and **2** (B) on the SiO_2 substrates.

2.6 *I-V* Properties

The porphyrin derivatives with uniform membrane structure would be promising candidates for applications in electronic devices. To demonstrate the potentials of these QLS films, these films were carefully transferred onto glass substrate with ITO interdigitated electrodes (IDEs). Fig. 6 shows the current-voltage (*I-V*) characteristics of the porphyrin derivatives of QLS films. The electronic conductivity is calculated to be around 1.5×10^{-2} $S\cdot m^{-1}$ and 2.7×10^{-3} $S\cdot m^{-1}$ respectively. It is noteworthy that the high electrical conductivity (ca. 10^{-2} ~ 10^{-3} $S\cdot m^{-1}$) has also been reported for nanobelts of the amphiphilic perylenetetracarboxylic diimide derivatives with the typical n-type character by several research groups,[35,36] which is attributed to ordered one-dimensional π-π stacking (cofacial π-electron delocalization). In the present case, the much higher conductivity in the QLS film of **1** compared to that of **2** might be due to the stronger intermolecular interactions and higher ordered crystalline molecular arrangement in the QLS film of **1**. These films with such high current modulation, could be useful for a wide range of electronic and sensor devices.

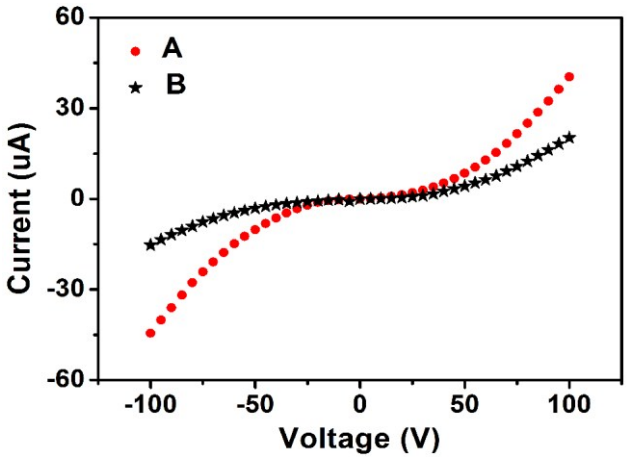

Fig. 6 *I-V* curves measured for the QLS films of **1** (A) and **2** (B) deposited on ITO IDEs/glass substrates, respectively.

2.7 Sensor performance measurement

Response of the QLS film-based sensors from **1** and **2** deposited onto the ITO IDEs/glass substrates were determined from the time-dependent current plots when exposed to NO_2 gas in the nitrogen at room temperature. As shown in Fig. 7A, when the QLS films of **1** were exposed to 200 and 800 ppm NO_2 (with a duty cycle where the dynamic exposure period is fixed at 4 min and the recovery period at 6 min), respectively, the conductivity decrease during exposure and increase to its initial value during recovery, indicating a good reversibility characteristic in the films. The similar behavior has already been observed in cobalt phthalocyanine[37] and bis(phthalocyaninato) holmium.[38] Similar response had been observed for film of 2, but the result is poorer with a slow duty cycle of 7 min/7 min. Considering the 5,10,15,20-tetraphenylporphyrin compound as a p-type organic semiconductor has been reported by Checcoli and co-

workers,[39] the n-type sensing response to NO_2 of **1** and **2** unambiguously reveals the significant substituents effect on tuning the nature of porphyrin organic semiconductors. It is well known that, n-type porphrin-based films are easily oxidized by the electron-accepting gas, NO_2, forming charge-transfer complexes upon analyte (NO_2) binding to these films, which inject holes and decrease film currents.[40]

In order to quantitatively analyze the sensor responses, we define relative response intensity $S = (\Delta I/I_0) \times 100\%$, where I_0 is the baseline current value, and $\Delta I = I_g - I_0$; I_g is the current value when the NO_2 gas is switched on. The relative response intensities at 200 and 800 ppm are 74.7 % and 86.9 % for the film of **1**, and 19.6 % and 24.3 % for the film of **2**. The higher *S* value of the film of **1** is resulted from not only better film-quality with the stronger molecular interactions among the adjacent molecules in the film of **1**, but more importantly to smaller mismatch between low-lying LUMO energy level of **1** (-3.88 eV) and the work function of the ITO electrode (-4.5 eV)[41] that results a smaller energy barrier for electron injection. Note that there is a weak discrimination of the QLS film of **1** and **2** to the different concentrations of NO_2 (800, 400 to 200 ppm) in N_2. Similar response was also observed when the sensor operates in ambient air. The time-dependent current plots of the QLS films of **1** and **2** exposed to different concentrations of NO_2 from 800, 400 to 200 ppm in ambient air have been shown in Fig. S3 in ESI. Apart from drying the air, no further precautions were taken, showing that the fabricated sensor is selective for NO_2.[42]

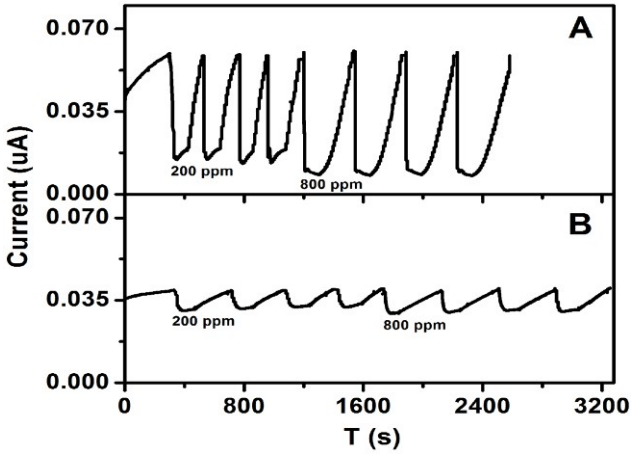

Fig. 7 The time-dependent current plots of the QLS films of **1** (A) and **2**) (B) exposed to NO_2 with the concentrations of 200 and 800 ppm for every four cycles, respectively.

3 Conclusion

In summary, two novel amphiphilic porphyrin zinc compounds with different hydrophilic polyoxyethylene substituents, [ZnT($OC_2H_4OC_2H_4OH$)PP] (**1**) and [ZnT(OC_2H_4NN15C5)PP] (**2**), have been designed, synthesized and fabricated into the QLS films to detect the NO_2 gas sensor properties at room temperature. UV-vis, XRD and AFM results suggest that the stronger intermolecular interaction with the π-π stacking interaction between tetrapyrrole rings in the porphyrin molecules of **1** than that of **2** leads to increased molecular packing and improved film-crystalinity. Correlatively, the conductivity of the QLS film of **1** is more than 1 order of magnitude higher than that of **2**. The more sensitive, stable and reproducible responses to NO_2 gas at the concentrations of 200 and 800 ppm are obtained for the film of **1** in a faster response/recovery cycle of only 4/6 min. Unexpectedly, a decreased current response towards NO_2 for the QLS films of both **1** and **2** were obtained for the first time, which unambiguously demonstrated the n-type semiconducting nature for **1** and **2**.

4 Experimental

4.1 Chemicals

All solvents were dried and distilled according to standard procedures. All other solvents and reagents such as $Zn(OAc)_2 \cdot 2H_2O$ were used as received. All air-sensitive reactions were carried out under nitrogen atmosphere. DMF and Dichloromethane were fresly distilled just before use. Column chromatography was carried out on silica gel (Merck, Kieselgel 60, 200-300 with mesh) the indicated eluent. 5-(Benzo-(4-(2-(2-hydroxy)ethoxy)ethoxy))-10,15,20-

triphenylporphyrinato zinc complex [ZnT($OC_2H_4OC_2H_4OH$)PP] (**1**) and 5-(4-(2-(4,10-N,N-15-Crown-5)ethoxy))-10,15,20-triphenylporphyrinato zinc complex [ZnT(OC_2H_4NN15C5)PP] (**2**) were synthesized and purified according to published procedures.[20] The detailed synthesis procedures together with the structural characterization are described in the ESI.*

4.2 Fabrication of the thin films

Thin films for device deposition was conducted as following: (i) quasi-Langmuir–Shäfer (QLS) film of [ZnT($OC_2H_4OC_2H_4OH$)PP] (**1**): Firstly, 5.0 mL of chloroform solution of [ZnT($OC_2H_4OC_2H_4OH$)PP] (**1**) (~1×10^{-6} mol·L^{-1}) was put into a cylindrical glass container (diameter: 9.5 cm, height: 1.5 cm, volume: 106.3 cm^3), then 65 mL of water was slowly added onto the container (caution: the amount of water added cannot cover completely surface of the chloroform solution so as to keep the path for the evaporation of the solvent, $CHCl_3$). During the solvent evaporation, the molecules gradually assembled to form some fine membrane structure at the $CHCl_3$/water interface and in turn the densely packed film on the water surface until complete evaporation of $CHCl_3$. The film can be easily transferred from the water surface onto ITO substrate by horizontal lifting, *i.e.* the slide was horizontally and carefully lowered onto the film surface and then raised.[20] This process was repeated to obtain the required number of layers. Residual water on the substrate, between transfer steps and after the final transfer, was removed with a stream of N_2. (ii) quasi-Langmuir–Shäfer (QLS) film of [ZnT(OC_2H_4NN15C5)PP] (**2**): It was fabricated according to QLS technology described above.[25]

4.3 Electrical experiments and measurements of NO_2 gas sensor

The fundamental electrical measurements were performed using a Hewlett-Packard (HP) 4140B parameter analyzer at room temperature. Current-voltage (*I-V*) curves were registered in the -100 to 100 V voltage range with 5 V increments, starting and finishing at 0 V bias to avoid irreversible polarization effects. All experiments have been conducted at least twice to ensure reproducibility. The interdigitated electrode array is composed of 10 pairs of ITO electrode digits deposited onto a glass substrate with the following dimensions: 125 μm electrode width, 75 μm spacing, 5850 μm overlapping length and 20 nm electrode thickness. Conductivity, σ can be calculated by the eqn (1),

$$\sigma = \frac{d \times I}{(2n-1) \times L \times h \times V} \qquad (1)$$

where d is the interelectrode spacing, I the current, n the number of electrode digits, L the overlapping length of the electrodes, and h the film thickness if it is less than that of the electrodes or the electrode thickness when the film thickness exceeds that of the ITO electrodes. The NO_2-sensing properties of samples have been examined by exposing the corresponding films to different concentrations of NO_2 gas and measuring the current changes of the films at a constantly polarized voltage of 9 V.

Acknowledgment

This work was financially supported by the National Natural Science Foundation of China (No. 21371073), Research Foundation from China University of Petroleum (East China) (Y1510051) and Shandong Academy of Agricultural Sciences Cooperation Guiding Plan Project (Grant No. 2014YDHZ04).

Additional file

Electronic Supplementary Information (ESI) available: Experimental isotopic pattern for the molecular ion of **1** (A) and **2** (B) shown in the MALDI–TOF mass spectrum. Polarized UV-vis spectra of compounds **1**-**2** (A-B) QLS films. The time-dependent current plots of the QLS films of **1** (A) and **2** (B) exposed to the different concentrations of NO_2 ranging from 800, 400 to 200 ppm in ambient air, respectively. See DOI: 10.1039/x0xx00000x.

Notes and references

1 F. Souza and O. Ito, Chem. Soc. Rev., 2012, 41, 86.
2 D. Gust, T. Moore and A. Moore, Acc. Chem. Res., 2009, 42, 1890.
3 E. Mal'tsev, M. Brusentseva, V. Rumyantseva, D. Lypenko, V. Berendyaev, A. Mironov, S. Novikov and A. Vannikov, Polym. Sci. A, 2006, 48, 146.
4 K. Peter, Palomaki, R. Marissa, and H. Peter, ACS Appl. Mater. Interfaces, 2013, 5, 7604.
5 V. Montes, C. Pérez-Bolívar, N. Agarwal, J. Shinar and P. Anzenbacher, J. Am. Chem. Soc., 2006, 128, 12436.
6 M. Seol, S. Choi, C. Kim, D. Moon and Y. Choi, ACS Nano, 2012, 6, 183.
7 S. Rao, N. Naga Srinivas, D. Rao, L. Giribabu, B. Maiya, R. Philip and G. Kumar, Opt. Commun., 2001, 192, 123.
8 F. Pavinatto, A. Gameiro Jr, A. Hidalgo, L. Dinelli, L. Romualdo, A. Batista, N. Barbosa Neto, M. Ferreira and O. Oliveira Jr, Appl. Surf. Sci., 2008, 254, 5946.
9 P. Ma, Y. Chen, Y. Bian and J. Jiang, Langmuir, 2010, 26, 3678.
10 X. Gong, T. Milic, C. Xu, J. Batteas and C. Drain, J. AM. Chem. Soc., 2002, 124, 14290.
11 G. Giancane and L. Valli, Advances in Colloid and Interface Science, 2012, 17–35, 171.
12 J. Pedrosa, C. Dooling, T. Richardson, R. Hyde, C. Hunter, M. MartÍn and L. Camacho, Materials Science and Engineering C, 2002, 22, 433.
13 K. Garg, A. Singh, C. Majumder, S. Nayak, D. Aswal, S. Gupta and S. Chattopadhyay, Organic Electronics, 2013, 14, 1189.
14 A. Dunbar, T. Richardson, J. Hutchinson, C. Hunter, Sensors and Actuators B, 2008, 128, 468.
15 A. D'Amicoa, C. Natalea, R. Paolesseb, A. Macagnanoa and A. Mantinia, Sensors and Actuators B, 2000, 65, 209.
16 S. Kladsomboon and T. Kerdcharoen, Analytica Chimica Acta, 2012, 757, 75.
17 Y. Chen, M. Bouvet, T. Sizun, Y. Gao, C. Plassard, E. Lesniewska and J. Jiang, Phys. Chem. Chem. Phys., 2010, 12, 12851.
18 J. Gao, G. Lu, J. kan, Y. Chen, M. Bouvet, Sensors and Actuators B: Chemical, 2012, 166–167, 500.
19 Y. Chen, M. Bouvet, T. Sizun, G. Barochi, J. Rossignol, E. Lesniewska, Sensors and Actuators B: Chemical, 2011, 155, 165.
20 G. Lu, Y. Chen, Y. Zhang, M. Bao, Y. Bian, X. Li and J. Jiang, J. AM. Chem. Soc., 2008, 130, 11623.
21 D. Li, H. Wang, J. Kan, W. Lu, Y. Chen and J. Jiang, Organic Electronics, 2013, 14, 2582.
22 G. Lu, X. Zhang, X. Cai and J. Jiang, J. Mater. Chem., 2009, 19, 2417.
23 A. Satake and Y. Kobuke, Org. Biomol. Chem., 2007, 5, 1679.
24 M. Kasha, H. Rawls and M. El-Bayoumi, Pure Appl. Chem., 1965, 11, 371.
25 Y. Chen, M. Bouvet, T. Sizun, G. Barochi, J. Rossignol and E. Lesniewska, Sens. Actuators B: Chem., 2011, 155, 165.
26 (a) M. Yoneyama, M. Sugi, M. Saito, K. Ikegami, S. Kuroda and S. Iizima, Jpn. J. Appl. Phys., 1986, 25, 961. (b) J. Bourgoin, F. Doublet, S. Palacin and M. Vandevyver, Langmuir, 1996, 12, 6473. (c) H. Xiang, K. Tanaka, A. Takahara and T. Kajiyama, Langmuir, 2002, 18, 2223.
27 H. Katz and Z. Bao, J. Phys. Chem. B, 2000, 104, 671.
28 N. An, Y. Shi, J. Feng, D. Li, J. Gao, Y. Chen and X. Li, Organic Electronics, 2013, 14, 1197.
29 J. Hill, W. Jin, A. Kosaka, T. Fukushima, H. Ichihara, T. Shimomura, K. Ito, T. Hashizume, N. Ishii and T. Aida, Science, 2004, 304, 1481.
30 Y. Yamamoto, T. Fukushima, Y. Suna, N. Ishii, A. Saeki, S. Seki, S. Tagawa, M. Taniguchi, T. Kawai and T. Aida, Science, 2006, 14, 1761.
31 Y. Gao, X. Zhang, C. Ma, X. Li and J. Jiang, J. AM. Chem. Soc., 2008, 130, 17044.
32 P. Ma, Z. Bai, Y. Gao, Q. Wang, J. Kan, Y. Bian and J. Jiang, Soft Matter, 2011, 7, 3417.
33 (a) J. Liu, K. Yang and Z. Lu, J. Am. Chem. Soc., 1997, 119, 11061. (b) T. Yamamoto, H. Kokubo, M. Kobubo, M. Kobashi and Y. Sakai, Chem. Mater., 2004, 16, 4616.
34 M. Kimura, T. Muto, H. Takimoto, K. Wada, K. Ohta, K. Hanabusa, H. Shirai and K. Nagao, Langmuir, 2000, 16, 2078.
35 Y. Che, A. Datar, X. Yang, T. Naddo, J. Zhao, and L. Zang. J. Am. Chem. Soc. 2007, 129, 6354-6355.
36 Y. Chen, Y. Feng, J. Gao, M. Bouvet, Journal of Colloid and Interface Science, 2012, 368, 387.
37 T. Sizun, M. Bouvet, Y. Chen, J. Suisse, G. Barochi and J. Rossignol, Sensors and Actuators B: Chemical, 2011, 159, 163.
38 Y. Chen, D. Li, N. Yuan, J. Gao, R. Gu, G. Lu and M. Bouvet, J. Mater. Chem., 2012, 22, 22142.
39 P. Checcoli, G. Conte, S. Salvatori, R. Paolesse, A. Bolognesi, M. Berliocchi, F. Brunetti, A. D'Amico, A. Carlo and P. Lugli, Synth. Met., 2003, 138, 261.
40 F. Bohrer, A. Sharoni, C. Colesniuc, J. Park, I. Schuller, A. Kummel and W. Trogler, J. Am. Chem. Soc., 2007, 129, 5640.
41 H. Yan, P. Lee, N. Armstrong, A. Graham, G. Evmenenko, P. Dutta and T. Marks, J. AM. Chem. Soc., 2005, 127, 3172.
42 A. Andringa, C. Piliego, I. Katsouras, P. Blom and D. Leeuw, Chem. Mater., 2014, 26, 773.

Table of Contents

Amphiphilic Unsymmetrically-Substituted Porphyrin Zinc Derivatives： Synthesis, Aggregation Behavior in the Self-Assemblied Films and NO_2 Sensing Properties

Yanling Wu,[a] Pan Ma,[c] Shanshan Liu[a] and Yanli Chen[a,b*]

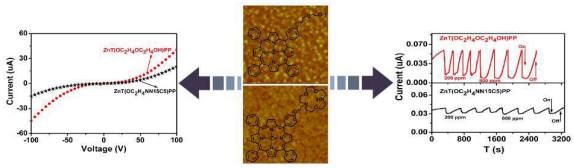

The first example of *n*-type amphiphilic metalloporphyrin-based semiconductors has been obtained as the NO_2 sensors.